Journal of Mathematical Control Science and Applications
Vol. 5 No. 1 (January-June, 2019)

MUK PUBLICATIONS
Open Access Publisher

Two-fluid Non-linear Models for Blood Flow in Stenosed Arteries: A Comparative Study

D. S. Sankar*

Abstract: Pulsatile flow of blood through stenosed arteries is analyzed by assuming the blood as a two-fluid model with the suspension of all the erythrocytes in the core region as a non-Newtonian fluid and the plasma in the peripheral layer as a Newtonian fluid. The non-Newtonian fluid in the core region of the artery is assumed as a (i) Herschel-Bulkley fluid and (ii) Casson fluid. Perturbation method is used to solve the system of non-linear partial differential equations. The expressions for velocity, flow rate, plug core radius, wall shear stress and resistance to flow are obtained for two-fluid Casson model and the expressions for these flow quantities obtained by Sankar and Lee (2006) for two-fluid Herschel-Bulkley model are used to get the data for comparison. It is noted that the plug flow velocity and velocity distribution for the two-fluid Casson model are considerably higher than those of the two-fluid Herschel-Bulkley model for a given set of values of the parameters. Further, it is found that the pressure drop, plug core radius, wall shear stress and the resistance to flow are significantly very low for the two-fluid Casson model than those of the two-fluid Herschel-Bulkley model. Thus, it is concluded that the two-fluid Casson model is more useful than the two-fluid Herschel-Bulkley model to analyze the blood flow through stenosed arteries.

Keywords: Two-fluid models; Pulsatile flow; Stenosed arteries; Non-Newtonian fluids; Resistance to flow

1. INTRODUCTION

There are many evidences that vascular fluid dynamics plays a major role in the development and progression of arterial stenosis. Arteries are narrowed by the development of atherosclerotic plaques that protrude into the lumen, resulting arterial stenosis. When an obstruction developed in an artery, one of the most serious consequences is the increased resistance and the associated reduction of the blood flow to the particular vascular bed supplied by the artery. Thus, the presence of a stenosis leads to the serious circulatory disorder.

Several theoretical and experimental attempts were made to study the blood flow characteristics in the presence of stenosis [1-8]. The assumption of Newtonian behavior of blood is acceptable for high shear rate flow through larger arteries [9]. But, blood, being a suspension of cells in plasma, exhibits non–Newtonian behavior at low shear rate ($\dot{\gamma} < 10$/sec) in small diameter arteries [10]. In diseased state, the actual flow is distinctly pulsatile [11, 12]. Many researchers studied the non–Newtonian behavior and pulsatile flow of blood through stenosed arteries [1, 3, 9, 12].

Bugliarello and Sevilla [13] and Cokelet [14] have shown experimentally that for blood flowing through narrow blood vessels, there is a peripheral layer of plasma and a core region of suspension of all the erythrocytes. Thus, for a realistic description of the blood flow, it is appropriate to treat blood as a two-fluid model with the suspension of all the erythrocytes in the core region as a non-Newtonian fluid and plasma in the peripheral region as a Newtonian fluid.

---

* School of Applied Sciences and Mathematics, Universiti Teknologi Brunei, Jalan Tungku Link Gadong BE 1410, Brunei Darussalam

Sankar and Lee [15] have developed two-fluid model for pulsatile blood flow through arterial stenosis treating the fluid in the core region as Herschel-Bulkley fluid. Thus, in this paper, we extend this study to two-fluid Casson model and; compare these models and discuss the advantages of the two-fluid Casson model over the two-fluid Herschel-Bulkley (H-B) model.

2. MATHEMATICAL FORMULATION

Consider an axially symmetric, laminar, pulsatile and fully developed flow of blood (assumed to be incompressible) in the $\bar{z}$ direction through a rigid walled circular artery with an axially symmetric mild stenosis. The geometry of the arterial stenosis is shown in Fig. 1. We have used the cylindrical polar coordinates ($\bar{r}$, $\bar{\phi}$, $\bar{z}$). Blood is represented by a two-fluid model with the suspension of all the erythrocytes in the core region as a Non-Newtonian fluid and the plasma in the peripheral region as a Newtonian fluid. The non-Newtonian fluid in the core region is represented by (i) Casson fluid model and (ii) Herschel-Bulkley fluid model. The geometry of the stenosis in the peripheral region (in dimensionless form) and core region are respectively given by

$$\bar{R}(z) = \begin{cases} \bar{R}_0 & \text{in the jormal artery region} \\ \bar{R}_0 - (\bar{\delta}_P/2)\left[1+\cos\left(2\pi/\bar{L}_0\right)\left\{\bar{z}-\bar{d}-\left(\bar{L}_0/2\right)\right\}\right] & \text{in } \bar{d} \le \bar{z} \le \bar{d}+\bar{L}_0 \end{cases} \tag{1}$$

$$\bar{R}_1(z) = \begin{cases} \beta\bar{R}_0 & \text{in the normal artery region} \\ \beta\bar{R}_0 - (\bar{\delta}_C/2)\left[1+\cos\left(2\pi/\bar{L}_0\right)\left\{\bar{z}-\bar{d}-\left(\bar{L}_0/2\right)\right\}\right] & \text{in } \bar{d} \le \bar{z} \le \bar{d}+\bar{L}_0 \end{cases} \tag{2}$$

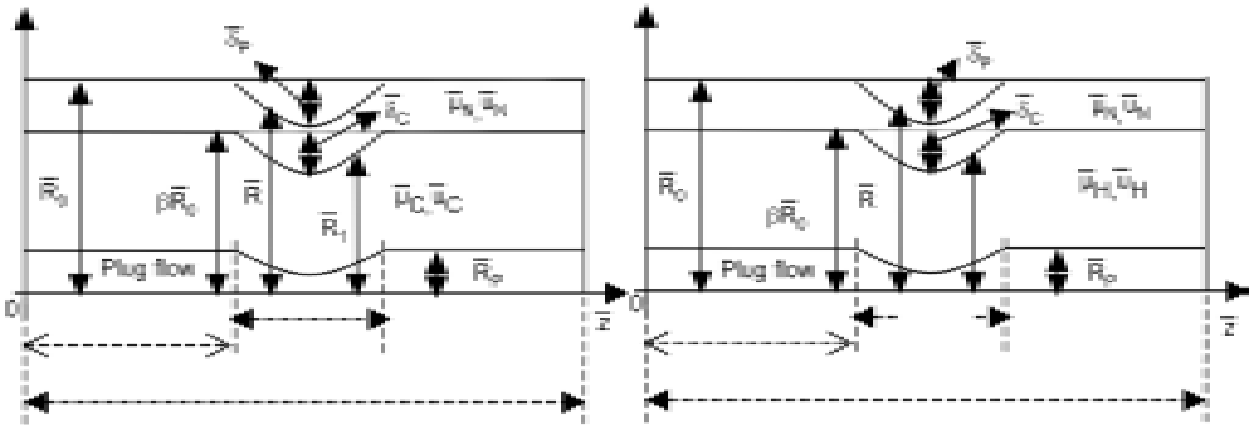

(a) Two-fluid Casson Model **(b) Two-fluid Herschel-Bulkley Model**

Figure 1: Geometry of the Two-fluid Models with Arterial Stenosis

where $\bar{R}(z)$ and $\bar{R}_1$ are the radii of the stenosed artery with the peripheral region and core region respectively; $\bar{R}_0$ and $\beta\bar{R}_0$ are the radii of the normal artery and core region of the normal artery respectively; β is the ratio of the central core radius to the normal artery radius; $\bar{L}_0$ is the length of the stenosis; $\bar{d}$ indicates the location of the stenosis; $\bar{\delta}_p$ and $\bar{\delta}_C$ are the maximum projections of the stenosis in the peripheral region and core region respectively such that $[\bar{\delta}_p/\bar{R}_0] << 1$ and $[\bar{\delta}_C/\bar{R}_0] << 1$.

2.1 TWO-FLUID CASSON MODEL

2.1.1 Governing equations

It can be shown that the radial velocity is negligibly small and can be neglected for a low Reynolds number flow. The basic momentum equations governing the flow are

$$\bar{\rho}_C\left(\partial\bar{u}_C/\partial\bar{t}\right) = -\left(\partial\bar{p}/\partial\bar{z}\right)-\left(1/\bar{r}\right)\left(\partial\left(\bar{r}\,\bar{\tau}_C\right)/\partial\bar{r}\right)\text{in } 0\le\bar{r}\le\bar{R}_1\left(\bar{z}\right) \tag{3}$$

$$\bar{\rho}_N\left(\partial\bar{u}_N/\partial\bar{t}\right) = -\left(\partial\bar{p}/\partial\bar{z}\right)-\left(1/\bar{r}\right)\left(\partial\left(\bar{r}\,\bar{\tau}_N\right)/\partial\bar{r}\right)\text{in } \bar{R}_1\left(\bar{z}\right)\le\bar{r}\le\bar{R}\left(\bar{z}\right) \tag{4}$$

where the shear stress $\bar{\tau} = |\bar{\tau}_{\bar{r}\bar{z}}| = -\bar{\tau}_{\bar{r}\bar{z}}$ (since $\bar{\tau} = \bar{\tau}_C$ or $\bar{\tau} = \bar{\tau}_N$); $\bar{p}$ is the pressure; $\bar{u}_C$ and $\bar{u}_N$ are the axial velocity of the fluid in the core region and peripheral region, respectively; $\bar{\tau}_C$ and $\bar{\tau}_N$ are the shear stress of the Casson fluid and Newtonian fluid, respectively; $\bar{\rho}_C$ and $\bar{\rho}_N$ are the densities of the Casson fluid and Newtonian fluid respectively; $\bar{t}$ is the time. The relations between the shear stress and strain rate of the fluids in motion in the core region (Casson fluid) and peripheral region (Newtonian fluid) are given by

$$\sqrt{\bar{\tau}_C} = \sqrt{-\bar{\mu}_C\left(\partial\bar{u}_C/\partial\bar{r}\right)}+\sqrt{\bar{\tau}_y}\ \text{if}\ \bar{\tau}_C\ge\bar{\tau}_y\ \text{and}\ \bar{R}_p\le\bar{r}\le\bar{R}_1\left(\bar{z}\right) \tag{5}$$

$$\left(\partial\bar{u}_C/\partial\bar{r}\right)=0 \quad \text{if} \quad \bar{\tau}_C\le\bar{\tau}_y \quad \text{and} \quad 0\le\bar{r}\le\bar{R}_p \tag{6}$$

$$\bar{\tau}_N = -\bar{\mu}_N\left(\partial\bar{u}_N/\partial\bar{r}\right) \quad \text{if} \quad \bar{R}_1\left(\bar{z}\right)\le\bar{r}\le\bar{R}\left(\bar{z}\right) \tag{7}$$

where $\bar{\mu}_C$ and $\bar{\mu}_N$ are the viscosities of the Casson and Newtonian fluids respectively; $\bar{\tau}_y$ is the yield stress; $\bar{R}_P$ is the plug core radius. The boundary conditions are

$$\begin{aligned}
&\bar{\tau}_C \quad \text{is finite and } \partial\bar{u}_C/\partial\bar{r}=0 \quad \text{at} \quad \bar{r}=0\\
&\bar{u}_N=0 \quad \text{at} \quad r=\bar{R}\\
&\bar{\tau}_C=\bar{\tau}_N \quad \text{and} \quad \bar{u}_C=\bar{u}_N \quad \text{at} \quad \bar{r}=\bar{R}_1
\end{aligned} \tag{8}$$

Since the pressure gradient is a function of $\bar{z}$ and $\bar{t}$, we assume

$$-\left(\partial\bar{p}/\partial\bar{z}\right)=\bar{q}\left(\bar{z}\right)f\left(\bar{t}\right) \tag{9}$$

where $\bar{q}\left(\bar{z}\right)=-\left(\partial\bar{p}/\partial\bar{z}\right)\left(\bar{z},0\right)$. Since, any periodic function can be expanded in a Fourier sine series, it is reasonable to choose $1+A\sin\bar{\omega}\bar{t}$ as a good approximation for $f(\bar{t})$, where A and $\bar{\omega}$ are the amplitude and angular frequency of the flow respectively. We introduce the following non-dimensional variables

$$z=\bar{z}/\bar{R}_0, R\left(z\right)=\bar{R}\left(\bar{z}\right)/\bar{R}_0, R_1\left(z\right)=\bar{R}_1\left(\bar{z}\right)/\bar{R}_0, r=\bar{r}/\bar{R}_0, d=\bar{d}/\bar{R}_0, L_0=\bar{L}_0/\bar{R}_0,$$

$$q\left(z\right)=\bar{q}\left(\bar{z}\right)/\bar{q}_0, \varepsilon_C=\alpha_C^2=\bar{R}_0^2\bar{\omega}\bar{\rho}_C/\bar{\mu}_C, \varepsilon_N=\alpha_N^2=\bar{R}_0^2\bar{\omega}\bar{\rho}_N/\bar{\mu}_N, R_P=\bar{R}_P/\bar{R}_0,$$

$$\delta_P=\bar{\delta}_P/\bar{R}_0, \delta_C=\bar{\delta}_C/\bar{R}_0, u_C=\bar{u}_C/\left(\bar{q}_0\bar{R}_0^2/4\bar{\mu}_C\right), u_N=\bar{u}_N/\left(\bar{q}_0\bar{R}_0^2/4\bar{\mu}_N\right),$$

$$\tau_C=\bar{\tau}_C/\left(\bar{q}_0\bar{R}_0/2\right), \tau_N=\bar{\tau}_N/\left(\bar{q}_0\bar{R}_0/2\right), \theta=\bar{\tau}_y/\left(\bar{q}_0\bar{R}_0/2\right), t=\bar{\omega}\bar{t} \tag{10}$$

where $\overline{q}_0$ is the negative of the pressure gradient in the normal artery, a_C and a_N are the pulsatile Reynolds numbers of the Casson fluid and Newtonian fluid respectively. Using the non-dimensional variables, Eqs. (1) - (5) are simplified to

$$\varepsilon_C\left(\partial u_C/\partial t\right)=4q(z)f(t)-(2/r)\partial\left(r\tau_C\right)/\partial r \quad \text{if } 0\le r\le R_1(z) \tag{11}$$

$$\sqrt{\tau_C}=\sqrt{(-1/2)\partial u_C/\partial r}+\sqrt{\theta} \quad \text{if } \tau_C\ge\theta \quad \text{and } R_p\le r\le R_1(z) \tag{12}$$

$$\partial u_C/\partial r=0 \quad \text{if } \tau_C\le\theta \text{ and } 0\le r\le R_p \tag{13}$$

$$\left.\begin{aligned}&\varepsilon_N\,\partial u_N/\partial t=4q(z)f(t)-(2/r)\partial\left(r\tau_N\right)/\partial r\\&\tau_N=-(1/2)\left(\partial u_N/\partial r\right)\end{aligned}\right\}\text{if} R_1(z)\le r\le R(z) \tag{14}$$

where

$$f(t) = 1 + A\sin t \tag{15}$$

The boundary conditions (in the dimensionless form) are

$$\begin{gathered}\tau_C \text{ is finite and } \partial u_C/\partial r = 0 \text{ at } r = 0\\ \tau_C = \tau_N \text{ and } u_C = u_N \text{ at } r = R_1\\ u_N = 0 \text{ at } r = R\end{gathered} \tag{16}$$

The geometry of the stenosis in the peripheral region and core region (in the dimensionless form) are given by

$$R(z)=\begin{cases}1 & \text{in the normal artery region}\\ 1-(\delta_P/2)\left\{1+\cos\left[(2\pi/L_0)\left(z-d-(L_0/2)\right)\right]\right\} & \text{in} \quad d\le z\le d+L_0\end{cases} \tag{17}$$

$$R_1(z)=\begin{cases}\beta & \text{in the normal artery region}\\ \beta-(\delta_C/2)\left\{1+\cos\left[(2\pi/L_0)\left(z-d-(L_0/2)\right)\right]\right\} & \text{in} \quad d\le z\le d+L_0\end{cases} \tag{18}$$

The non-dimensional volume flow rate Q is given by

$$Q=4\int_0^{R(z)}u(r,z,t)\,r\,dr \tag{19}$$

where $Q=\overline{Q}/(\pi\overline{R}_0^4\overline{q}_0/8\overline{\mu}_0)$, $\overline{Q}$ is the volume flow rate.

2.1.2 Method of Solution

When we non-dimensionalize the constitutive Eqs. (1) and (2), ε_C and ε_N occur naturally and these are time dependent and hence, it is more appropriate to expand the Eqs. (11)-(14) about ε_C and ε_N. Let us expand the plug core velocity u_p, the velocity in the core region u_C in the perturbation series of ε_C as below (where $\varepsilon_C << 1$)

$$u_p(z,t) = u_{op}(z,t) + \varepsilon C\, u_{1p}(z,t) + \ldots \tag{20}$$

$$u_C(r,z,t) = u_{0C}(r,z,t) + \varepsilon_C\, u_{1C}(r,z,t) + \ldots \tag{21}$$

Similarly, one can expand u_N, τ_P, τ_C, τ_N and R_P in powers of ε_C and ε_N, where $\varepsilon_N << 1$. Using the perturbation series in Eqs. (11) and (12) and then equating the constant terms and ε_C terms, the differential equations of the core region become

$$\begin{aligned} \partial\left(r\tau_{0C}\right)/\partial r &= 2q(z)f(t)r, & \partial u_{0C}/\partial t &= -(2/r)\,\partial\left(r\tau_{1C}\right)/\partial r \\ -\partial u_{0C}/\partial r &= 2\left(\tau_{0C} - 2\sqrt{\theta\tau_{0C}} + \theta\right), & -\partial u_{1C}/\partial r &= 2\tau_{1C}\left(1-\sqrt{\theta/\tau_{0C}}\right) \end{aligned} \tag{22}$$

Similarly, using the perturbation series expansions in Eq. (14) and then equating the constant terms and ε_N terms, the differential equations of the peripheral region become

$$\begin{aligned} \partial\left(r\tau_{0N}\right)/\partial r &= 2q(z)f(t)r, & \partial u_{0N}/\partial t &= -(2/r)\,\partial\left(r\tau_{1N}\right)/\partial r \\ -\partial u_{0N}/\partial r &= 2\tau_{0N}, & -\partial u_{1N}/\partial r &= 2\tau_{1N} \end{aligned} \tag{23}$$

Substituting the perturbation series expansions in Eq. (16) and then equating the constant terms and ε_C and ε_N terms, we get

$$\begin{aligned} &\tau_{0p} \text{ and } \tau_{1p} \text{ are finite and } \partial u_{0P}/\partial r = 0, \partial u_{1P}/\partial r = 0 \text{ at } r = 0 \\ &\tau_{0C} = \tau_{0N}, \tau_{1C} = \tau_{1N}, u_{0C} = u_{0N}, u_{1C} = u_{1N} \text{ at } r = R_1 \\ &u_{0N} = u_{1N} = 0 \text{ at } r = R \end{aligned} \tag{24}$$

Solving the system of Eqs. (22) and (23) using Eq. (24) for the unknowns u_{0C}, u_{1C}, τ_{0C}, τ_{1C}, u_{0N}, u_{1N}, τ_{0N}, τ_{1N}, one can obtain

$$\tau_{0p} = \nabla R_{0p},\ \tau_{0C} = ,\ \nabla r,\ \tau_{0N} = \nabla r \tag{25}$$

$$u_{0N} = \nabla\, R^2\,(1-\ \xi^2) \tag{26}$$

$$u_{0C} = \nabla R^2\,\{(1-\Omega^2) + \Omega^2\,[(1-\xi_1^{\,2}) - (8/3)\,\sigma_1^{\,1/2}\,(1-\sigma_1^{\,3/2}) + 2\sigma_1\,(1-\xi_1)]\} \tag{27}$$

$$u_{0p} = \nabla R^2\,\{(1-\Omega^2) + \Omega^2\,[(1-\chi^2) - (8/3)\,\sigma_1^{\,1/2}\,(1-\chi^{3/2}) + 2\sigma_1\,(1-\chi)]\} \tag{28}$$

$$\tau_{1p} = \nabla BR^3\,\{(1/4)\sigma(1-\Omega^2) + \Omega^3\,\sigma_1[(1/4) - (1/3)\,\sigma_1^{\,1/2} + (1/12)\,\sigma_1^{\,2}]\} \tag{29}$$

$$\begin{aligned} \tau_{1C} = &-\nabla\, BR^3\,\{(1/4)\xi\,(1-\Omega^2) \\ &-(1/8)\Omega^3\,[2\xi_1 - \xi_1^{\,3} - \sigma_1^{\,4}\,\xi_1^{\,-1} - (8/21)\sigma_1^{\,1/2}\,(7\xi_1 - 4\xi_1^{\,5/2} - 3\sigma_1^{\,7/2}\,\xi_1^{\,-1})]\} \end{aligned} \tag{30}$$

$$\begin{aligned} \tau_{1N} = &-\nabla\, BR^2\,R_1\,\{([1/4)\xi_1 - (1/8)\Omega^2\,\xi_1^{\,-1} - (1/8)\Omega^2\xi_1^{\,3}] \\ &+\xi_1^{\,-1}\,\Omega^2\,[(1/8) - (1/7)\,\sigma_1^{\,1/2} + (1/56)\sigma_1^{\,4}]\} \end{aligned} \tag{31}$$

$$\begin{aligned} u_{1N} = &-\nabla\, BR^3\,R_1\,\{[1/4)\,\Omega^{-1}\,(1-\xi^2) - (1/4)\Omega^3\log\xi^{-1} - (1/16)\,\Omega^{-1}\,(1-\xi^4)] \\ &-\Omega^3\log\xi\,[(1/4) - (2/7)\,\sigma_1^{\,1/2} + (1/28)\sigma_1^{\,4}]\} \end{aligned} \tag{32}$$

$$\begin{aligned} u_{1C} = &-\nabla\, BR^3\,R_1\,\{[3/16)\Omega^{-1} - (1/4)\Omega + (1/16)\Omega^3 + (1/4)\Omega^3\log\Omega] \\ &-\Omega^3\log\Omega\,[(1/4(- (2/7)\sigma_1^{\,1/2} + (1/28)\sigma_1^{\,4}] \\ &+\Omega\,(1-\Omega^2)[(1/4)(1-\xi_1^{\,2}) - (1/3)\sigma_1^{\,1/2}\,(1-\xi_1^{\,3/2})] \\ &+\Omega^3\,[(1/4)\,(1-\xi_1^{\,2}) - (1/3)\sigma_1^{\,1/2}\,(1-\xi_1^{\,3/2}) - (1/16)(1-\xi_1^{\,4}) \\ &+(53/294)\sigma_1^{\,1/2}\,(1-\xi_1^{\,7/2}) - (1/3)\,(1-\xi_1^{\,2}) + (4/9)\,\sigma_1\,(1-\xi_1^{\,3/2}) \end{aligned} \tag{33}$$

$$
\begin{aligned}
&-(8/63)\sigma_1\,(1-\xi_1{}^3)-(1/28)\sigma_1{}^4\log\xi^1+(1/14)\sigma_1{}^{9/2}\,(1-\xi_1{}^{-1/2})]\}\\
u_{1P}\;&=-\nabla\,BR^3\,R1\,\{((3/16)\Omega^{-1}-(1/4)\Omega+(1/16)\Omega^3+(1/4)\Omega^3\log\Omega)\\
&\quad-\Omega^3\log\Omega\,((1/4)-(2/7)\sigma_1{}^{1/2}+(1/28)\,\sigma_1{}^4)\\
&\quad+\Omega\,(1-\Omega^2)[1/4)(1-\sigma_1{}^2)-(1/3)\,\sigma_1{}^{1/2}\,(1-\sigma_1{}^{3/2})]\\
&\quad+\Omega^3\,[(1/4)(1-\sigma_1{}^2)-(1/3)\sigma_1{}^{1/2}\,(1-\sigma_1{}^{3/2})-(1/16)\,(1-\sigma_1{}^4)\\
&\quad-(53/294)\sigma_1{}^{1/2}\,(1-\sigma_1{}^{7/2})-(1/3)(1-\sigma_1{}^2)+(4/9)\,\sigma_1\,(1-\sigma_1{}^{3/2})\\
&\quad+(8/63)\,2\sigma_1\,(1-\sigma_1{}^3)-(1/28)\,\sigma_1{}^4\log\sigma_1+(1/14)\,\sigma_1{}^{9/2}\,(1-\sigma_1{}^{-1/2})]\}
\end{aligned}
\tag{34}
$$

where $\nabla = q(z)f(t)$, $k^2 = r|r_{0p^z\,\theta} = R_{0p} = \theta\,/\,[q(z)f(t)]$, $B = [1/f(t)](df(t)/dt)$, $\xi = r/R$, $\xi_1 = r/R_1$, $\Omega = R_1/R$, $\sigma = k^2/R$, $\sigma_1 = k^2/R_1$, and $\chi = R_{0p}/R_1$. The wall shear stress τ_w can be obtained as below.

$$
\begin{aligned}
\tau_w &= (t_{0N} + \varepsilon_N\tau_{1N})_{r=R} = \tau_{0w} + \varepsilon_N\,\tau_{1w}\\
&= \nabla\,\{R - 1/8)\,BR^3\,\varepsilon_N\,(1-\Omega^4) - (1/8)\,BR_1{}^3\,\varepsilon_N\,\Omega\,[1-(8/7)\,\sigma_1{}^{1/2} + (1/7)\,\sigma_1{}^4]\}
\end{aligned}
\tag{35}
$$

Using Eqs. (26)-(28) and (32)-(34) in Eq. (19), the volume flow rate is obtained as

$$
\begin{aligned}
Q &= \nabla\,R^4\,\{1-\Omega 2)\,(1+3\Omega^2)+\Omega^4\,[1-(16/7)\sigma_1{}^{1/2}+(4/3)\sigma_1-(1/21)\sigma_1{}^4]\}\\
&\quad-\varepsilon_C\,\nabla\,BR3\,R_1{}^3\,\{[3/8)\Omega^{-1}-(1/2)\Omega+(1/8)\Omega^3+(1/2)\,\Omega^3\log\Omega]\\
&\quad-\Omega^3\log\Omega\,[(1/2)-(4/7)\sigma_1{}^{1/2}+(1/14)\sigma_1{}^4]\\
&\quad+\Omega(1-\Omega_2)\,[(1/4)-(2/7)\sigma_1{}^{1/2}+(1/28)\,\sigma_1{}^4]\\
&\quad+\Omega^3\,[(1/6)-(30/77)\sigma_1{}^{1/2}+(8/35)\sigma_1-(1/3)\,\sigma_1{}^{3/2}+(1/14)\,\sigma_1{}^4\\
&\quad+(5/21)\,\sigma_1{}^{9/2}-(41/770)\,\sigma_1{}^6-(1/14)\,\sigma_1{}^6-\log\sigma_1+(1/14)\,\sigma_1{}^4\,(1-\sigma_1{}^2)\log k]\}\\
&\quad-\varepsilon_N\,\nabla\,BR^5\,R_1\,\{[(1/6)\Omega^{-1}-(3/8)\Omega+(5/24)\Omega^5-(1/2)\Omega3\,(1-\Omega^2)\log R_1]\\
&\quad+\Omega^4\,(1-\Omega^2)\,(1+2\log R_1)\,[(1/4)-(2/7)\,\sigma_1{}^{1/2}+(1/28)\,\sigma_1{}^4]\}
\end{aligned}
\tag{36}
$$

The shear stress $\tau_C = \tau_C + \varepsilon_H\,\tau_{1C}$ at $r = R_p$ is given by

$$
|\tau_{0C} + \varepsilon_C\,\tau_{1C}|_{r=R_p} = \theta \tag{37}
$$

Using the Taylor's series of τ_{0C} and τ_{1C} about R_{0p} and using $\tau_{0C}|_{r=R_{0p}} = \theta$, we get

$$
R_{1p} = -\,\tau_{1C}|_{r=R_{0P}}/\nabla \tag{38}
$$

Using Eqs. (25), (30) and (38) in the two term approximated perturbation series of R_P, the expression for R_p can be obtained as

$$
R_p = k^2 - (1/4)\,B\varepsilon_C\,R^3\,[\sigma^2\,(1-\Omega^2) + \Omega^3\,(\sigma_1 - 4\sigma_1{}^{3/2}/3 + \sigma_1{}^3/3)] \tag{39}
$$

The resistance to flow is given by

$$
\Lambda = [\Delta p\,f(t)]/Q \tag{40}
$$

where Δp is the pressure drop. When $R_1 = R$, the present model reduces to the single fluid Casson model and in such case, the expressions obtained in the present model for velocity u_C, shear stress τ_C, wall shear stress τ_w, flow rate Q and plug core radius R_p are in good agreement with those of Chaturani and Ponnalagar Samy [12].

2.2 Two-Fluid Herschel-Bulkley Model

The basic momentum equations governing the flow and the constitutive equations in the non-dimensional form are

$$\varepsilon_H (\partial u_H/\partial t) = 4q\,(z)\, f\,(t) - (2/r)(\partial(r\tau_H)/\partial r) \text{ if } 0 \le r \le R_1\,(z) \tag{41}$$

$$\varepsilon_H (\partial u_N/\partial t) = 4q\,(z)\, f(t) - 2/r)(\partial(r\tau_N)/\partial r) \text{ if } R_1(z) \le r \le R(z) \tag{42}$$

$$\tau_H = \sqrt[n]{-(1/2)(\partial u_H/\partial r)} + \theta \text{ if } \tau_H \ge \theta \text{ and } R_p \le r \le R_1(z) \tag{43}$$

$$\partial u_H/\partial r = 0 \text{ if } \tau_H \le \theta \text{ and } 0 \le r \le R_p \tag{44}$$

$$\tau_N = -\,(1/2)\,(\partial u_N/\partial r) \text{ if } R_1\,(z) \le r \le R(z) \tag{45}$$

The boundary conditions (in dimensionless form) of this model are similar to the boundary conditions of the two-fluid Casson model given in Eq. (8). Eqs. (41) – (45) are also solved using perturbation method with the help of the appropriate boundary conditions as in the case of the two-fluid Casson model. The details of the derivation of the expressions for shear stress, velocity, flow rate, plug core radius, wall shear stress and resistance to flow are given in Sankar and Lee [15].

3. RESULTS AND DISCUSSION

The objective of the present analysis is to compare and bring out advantages of the two-fluid Casson model over the two-fluid Herschel-Bulkley model. It is observed that the typical value of the power law index n for blood flow models is taken as 0.95 [3]. The value 0.1 used for the non-dimensional yield stress θ in this study. Though the range of the amplitude A is from 0 to 1, we have used the value 0.5. The value 0.5 is used for the pulsatile Reynolds number $\alpha_{H,}\,\alpha_C$ and pulsatile Reynolds number ratio α of both the two-fluid models [11]. The value of the ratio β of central core radius $\beta\,\bar{R}_0$ to the normal artery radius $\bar{R}_0$ in the unobstructed artery is generally taken as 0.95 [15]. Following Shukla et al. [16], relations $R_1 = \beta R$ and $\delta_c = \beta\delta_p$ are used to estimate R_1 and δ_c. The maximum thickness of the stenosis in the peripheral region δ_p is taken as 0.1 [11]. The steasy flow rate Q_S value is taken as 1.0 [12]. It is observed that in the expression of the flow rate for the two-fluid Casson model, $f(t)$, R and θ are known and Q and $q(z)$ are the unknowns to be determined. A careful analysis of the flow rate expression reveals the fact that $q(z)$ is the pressure gradient of the steady flow. Thus, if steady flow is assumed, then the expression for the flow rate can be solved for $q(z)$ [3,12]. For steady flow, the expression for flow rate of the two-fluid Casson model reduces to

$$\left(R^4 - 4R^2R_1^2 + 3R_1^4\right)y^4 + \left[\left(R_1 y\right)^4 - (16/7)\sqrt{\theta}\left(\sqrt{R_1 y}\right)^7 + (4/3)\theta\left(R_1 y\right)^3 - (1/21)\theta^4\right] - Q_S y^3 = 0 \tag{46}$$

The similar equation for the two-fluid Herschel-Bulkley model is

$$(R^2 - R_1^{\,2})\lfloor 4(\theta/\Omega)^2 + (R^2 - R_1^{\,2})\rfloor y^3 + [4/(n+2)(n+3)]$$
$$\{(n+2)(R_1 y)^{n+3} - n(n+3)\theta\,(R_{1y})^{n+2} + (n^2 + 2n - 2)\,\theta^{n+2}\} - Q_S\, y^3 = 0 \tag{47}$$

The variation of pressure drop in a time cycle for the two-fluid Herschel-Bulkley (H-B) and Casson models with $\theta = \delta_p = 0.1$, A = 0.5 and $\beta = 0.95$ is shown in Fig. 2. It is observed that for both the two-fluid models the pressure drop increases as time t (in degrees) increases from 0° to 90° and then it decreases as t increases from 90° to 270° and again the pressure drop increases as t increases further from 270° to 360°. The pressure drop is maximum at 90° and minimum at 270°. It is found that at any time, the pressure drop is considerably very low for the two-fluid Casson model than that of the two-fluid H-B model while all the other parameters held constant. Fig. 3 depicts the variation of the plug core radius with axial distance for the two-fluid H-B and Casson models with $\theta = \delta_p = 0.1$, A = 0.5 and $\beta = 0.95$. It is noticed that the plug core radius decreases as the axial variable

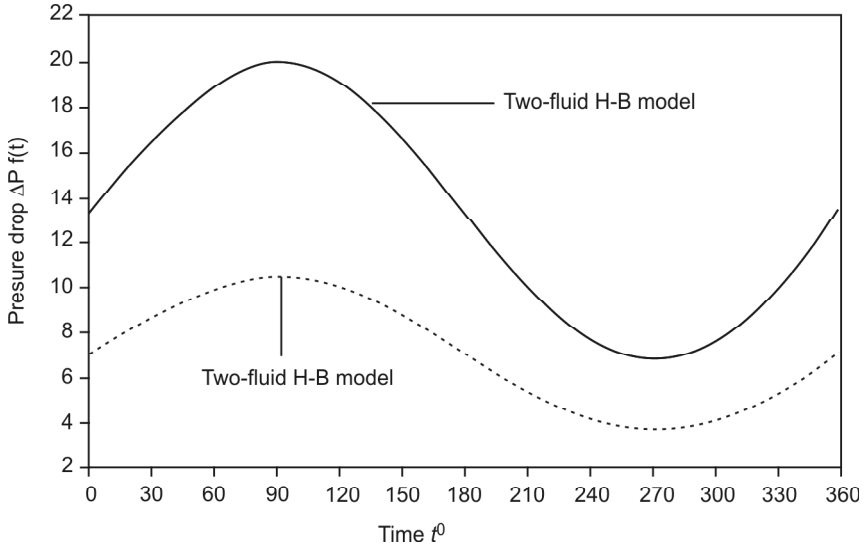

Figure 2: Variation of Pressure Drop in a Time Cycle for the Two-fluid Casson and H-B Models

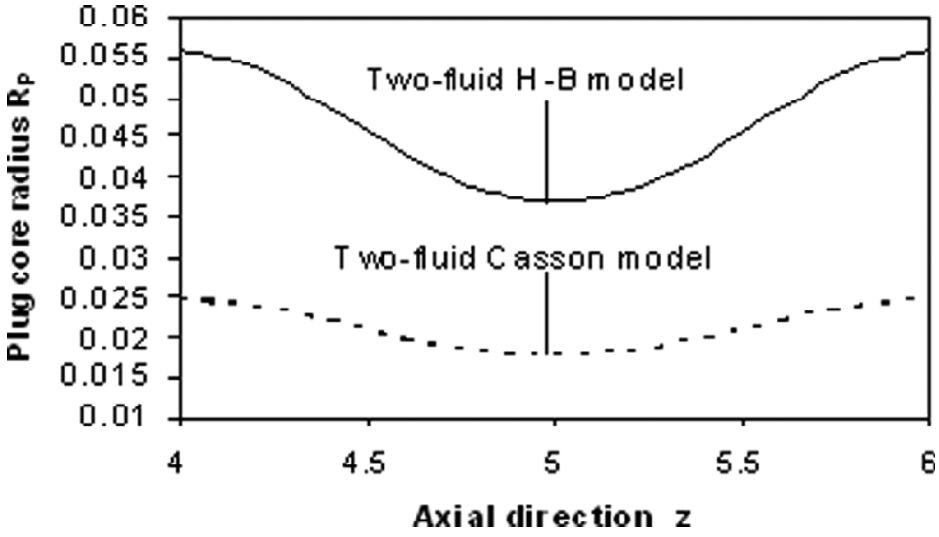

Figure 3: Variation of Plug Core Radius with Axial Distance for the Two-fluid Casson and Herschel-Bulkley Models

increases from 4 to 5 and it increases symmetrically when the axial variable increases from 5 to 6. It is noted that for a given set of values of the parameters, the plug core radius values are significantly very low for the two-fluid Casson model than that of the two-fluid H-B model.

3.1 Plug Flow Velocity

The variation of the plug flow velocity in a time cycle for the two-fluid Casson and H-B models with $\theta = \delta_P = 0.1$, $A = 0.5$, $\alpha = \alpha_H = \alpha_C = 0.5$, $\alpha_N = 0.25$, $\beta = 0.95$ and $z = 5$ is depicted in Fig. 4. It is seen that the plug flow velocity decreases as time t (in degrees) increases from 0° to 90° and then it increases as t increases from 90° to 270° and then again it decreases from 270° to 360°. The plug flow velocity is minimum at 90° and maximum at 270°. It is noted that the plug flow velocity is considerably higher for the two-fluid Casson model than that of the two-fluid H-B model.

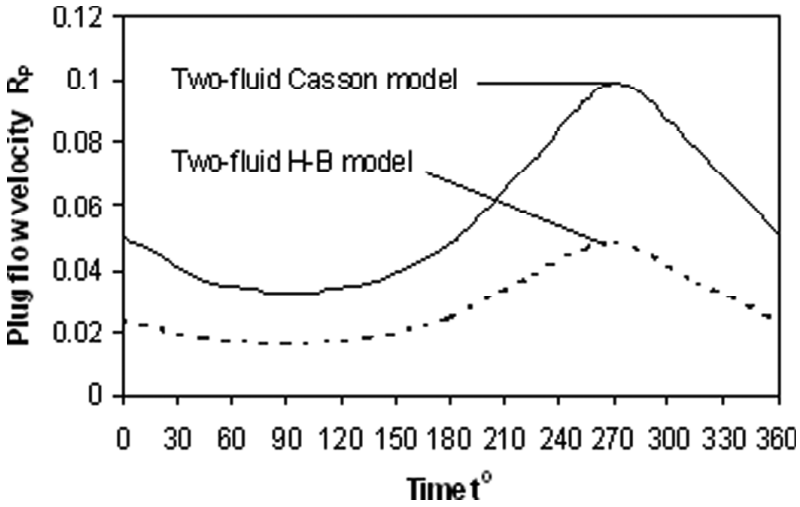

Figure 4: Variation of Plug Flow Velocity in a Time Cycle for the Two-fluid Casson and Two Fluid Herschel-Bulkley Models

3.2 Wall Shear Stress

Fig. 5 shows the variation of the wall shear stress in a time cycle for the two-fluid Casson and H-B models with $\theta = \delta_P = 0.1$, $A = 0.5$, $\alpha = \alpha_H = \alpha_C = 0.5$, $\alpha_N = 0.25$, $\beta = 0.95$ and $z = 5$. The behaviour of the wall shear stress is just reversed for the two-fluid models that we observed in Fig. 4 for the plug flow velocity.

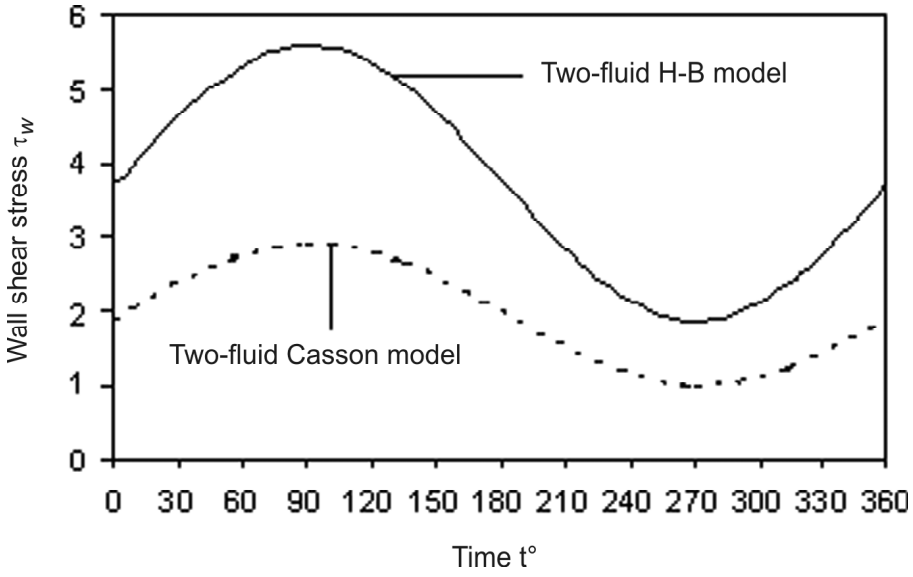

Figure 5: Variation of Wall Shear Stress in a Cycle for the Two-fluid Casson and Two Fluid Herschel-Bulkley Models

3.3 Velocity Distribution

The velocity distributions for the two-fluid H-B and Casson models with $\theta = \delta_P = 0.1$, $A = 0.5$, $\alpha = \alpha_H = \alpha_C = 0.5$, $\alpha_N = 0.25$, $\beta = 0.95$ and $t = 45°$ are sketched in Fig. 6. One can notice the plug flow around the tube axis for both the fluid models. It is further recorded that for a given set values of the parameters, a significantly high magituge velocity profile is found for the two-fluid Casson model model than the two-fluid H-B model.

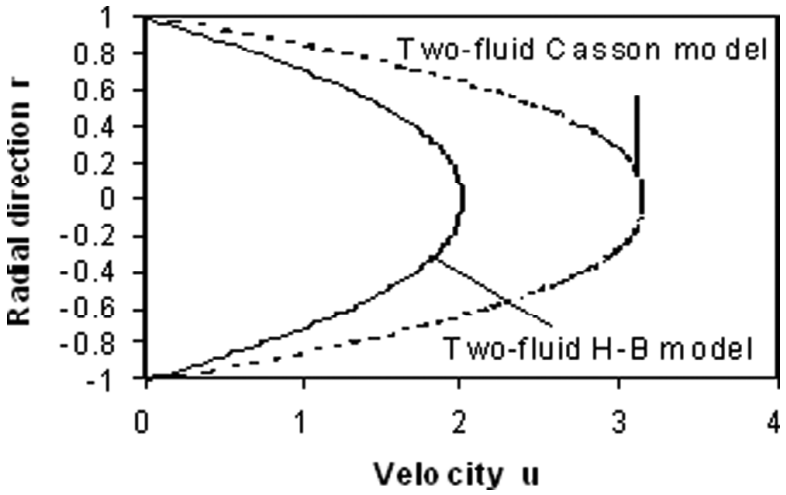

Figure 6: Velocity Distribution for the Two-fluid Casson and Two-fluid Herschel-Bulkley Model

3.4 Resistance to Flow

The variation of resistance to flow with peripheral layer stenosis height for the two-fluid Casson and H-B models with $\theta = \delta_P = 0.1$, $A = 0.5$, $a = a_H = a_C = 0.5$, $\alpha_N = 0.25$, $\beta = 0.95$ and $t = 45°$ is shown in Fig. 7. It is seen that the resistance to flow increases non-linearly with the increase of the peripheral stenosis height. It is of interest to note that for any value of the stenosis height, the resistanc to flow is considerably very low for the two-fluid Casson model than that of the H-B model.

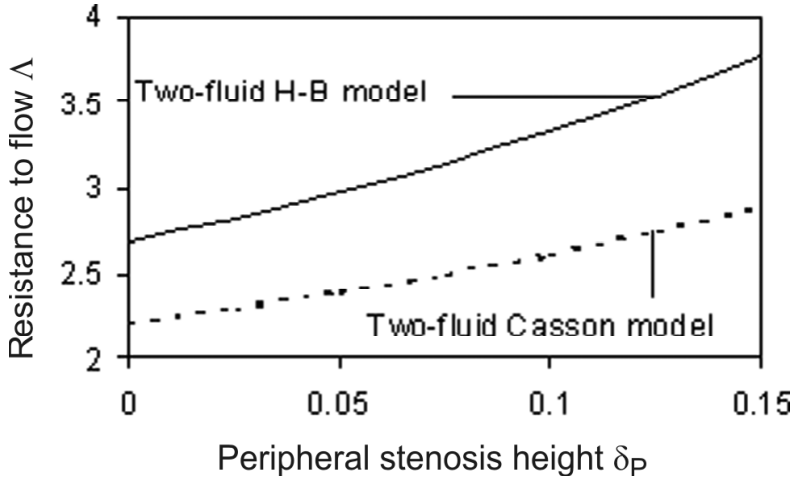

Figure 7: Variation of Resistance to Flow with Peripheral Layer Stenosis Height for the Two- fluid Casson and Two-fluid Herschel-Bulkley Models

4. CONCLUSION

The pulsatile blood flow through stenosed arteries is analyzed assuming blood as a (i) two-fluid Casson model and (ii) two-fluid Herschel-Bulkley model. It is observed that the velocity distribution for the two-fluid Casson model is considerably higher than that of the two-fluid Herschel-Bulkley fluid model for a given set of values of the parameters. Further, it is noticed that the pressure drop, plug core radius, wall sheat stress and the resistanc to flow are significantly very low for the two-fluid Casson model than those of the two-fluid Herschel-Bulkley

model. It is of interest to note that the difference between the estimates of the two-fluid Casson model and the two-fluid Herschel-Bulkley model is sustantial. Thus, it is concluded that the two-fluid Casson model will have more applicability in analysing the blood flow through stenosed arteries.

REFERENCES

[1] P. K. Mandal, An Unsteady analysis of non-Newtonian blood flow through tapered arteries with a stenosis, *Int. J. Non-Linear Mech.*, Vol. **40**, pp. 151–164, 2005.

[2] I. Marshall, S. Zhao, P. Papathanasopoulou, P. Hoskins and X. Y. Xu, MRI and CFD studies of pulsatile flow in healthy and stenosed carotid bifurcation models, *J. Biomech.,* Vol. **37**, pp. 679–687, 2004.

[3] D. S. Sankar and K. Hemalatha, Pulsatile flow of Herschel-Bulkey fluid through stenosed arteries - A mathematical model, *Int. J. Non-Linear Mech.,* Vol. **41**, pp. 979–990, 2006.

[4] M. S. Moayeri and G. R. Zendehbudi, Effects of elastic property of the wall on flow characteristics through arterial stenosis, *J. Biomech.,* Vol. **36**, pp. 525–535, 2003.

[5] S. Chakravarthy and P. K. Mandal, Two-dimensional blood flow through tapered arteries under stenotic conditions, *Int. J. Non-Linear Mech.*, Vol. **35**, pp. 779–793, 2000.

[6] G. T. Liu, Y. J. Wang, B. Q. Ai and L. G. Liu, Numerical study of pulsating flow through a tapered artery with stenosis, *Chinese J. Phys.*, Vol. **42**, pp. 401–409, 2004.

[7] Q. Long, X. Y. Ku, K. V. Ramnarine and P. Hoskins, Numerical investigations of physiologically realistic pulsatile flow through arterial stenosis, *J. Biomech.,* Vol. **34**, pp. 1229–1242, 2201.

[8] R. K. Dash, G. Jayaraman and K. N. Metha, Flow in a catheterized curved artery with stenosis, *J. Biomech.,* Vol. **32**, pp. 49–61, 1999.

[9] C. Tu and M. Deville, Pulsatile flow of non-Newtonian fluids through arterial stenosis, *J. Biomech.,* Vol. **29**, pp. 899 – 908, 1996.

[10] S. Chien, Hemorheology in Clinical Medicine, Recent Advances in Cardiovascular Diseases, Vol. **2**, pp. 21–26, 1981.

[11] V. P. Srivastava and M. Saxena, Two-Layered model of Casson fluid flow through stenotic blood vessels: Applications to the cardiovascular system, *J. Biomech.,* Vol. **27**, pp. 921–928, 1994.

[12] P. Chaturani and R. Ponnalagar Samy, Pulsatile flow of Casson's fluid through stenosed arteries with applications to blood flow, *Biorheology*, Vol. **23**, pp. 499–511, 1986.

[13] G. Bugliarello and J. Sevilla, Velocity distribution and other characteristics of steady and pulsatile blood flow in fine glass tubes, *Biorheology*, Vol. **7**, pp. 85–107, 1970.

[14] G. R. Cokelet, The rheology of human blood, Prentice-Hall, *Cliffs*, N.J., 1972.

[15] D. S. Sankar and U. Lee, Two-phase Non-linear Model for the Flow through Stenosed Blood Vessels, *KSME Journal of Mechanical Science and Technology*, Vol. **21**, pp. 678–689, 2007.

[16] J. B. Shukla, R. S. Parihar and S. P. Gupta, Effects of peripheral layer viscosity on blood flow through the artery with mild stenosis, *Bull. Math. Biol.*, Vol. **42**, pp. 797–805, 1980.